Ultrasound-assisted sol-gel synthesis, characterization, and photocatalytic application of ZnO nanoparticles

N. T. Nguyen[a*], V. A. Nguyen [b]
[a] *School of Chemical Engineering, Hanoi University of Science and Technology,*
[b] *Faculty of Natural Sciences and Technology, Hanoi Metropolitan University, Vietnam*

In this study we synthesized nano-sized ZnO particles by ultrasonic-assisted sol-gel method. The materials were, then, sintered at different temperatures of 400 ^{o}C, 500 ^{o}C, 600 ^{o}C, and 700 ^{o}C. The structural, morphological, and optical properties of the obtained ZnO nanoparticles were characterized by XRD, UV VIS, FE-SEM, and TEM. The results showed that ZnO nanoparticles have a hexagonal wurtzite crystalline structure, spherical and hexagonal shapes, and an average size of 22-30 nm. ZnO nanoparticles were used as photocatalysts to decompose methylene blue under ultraviolet light. The results showed that the materials are able to decompose methylene blue under ultra-violet lights. The material sintered 600^{o}C achieved the highest efficiency. From that, it can be concluded that ZnO nanoparticles have potential applications as photocatalysts for organic dyes removal in aqueous solutions.

(Received April 22, 2023; Accepted July 26, 2023)

Keywords: Zinc oxide, Nanoparticles, Ultrasound-assisted sol-gel, Photodegradation, Dye

1. Introduction

Since decades, the topic of nanomaterials has gained a lot of interest of scientists due to their special physical, chemical, and biological properties compared to bulk materials [1]. As a result, researchers around the world have continuously developed applications of nanomaterials in a wide range of scientific fields especially in environment field [2-4]. Among currently very diverse nanomaterials, ZnO nanoparticles are of particular interest thanks to advantages such as low cost, wide applicability, and especially environmental friendliness (physical and chemical stability, biocompatibility, and nontoxicity). As an important semiconductor with a wide bandgap (3.37eV) and a large exciton binding energy (60meV), ZnO nanoparticles are commonly selected to be a potential photocatalyst for pollutants removal [5, 6]. To be able to be applied in practice as photocatalysts, ZnO nanoparticles need to meet the following requirements: (1) high photosensitive activity; (2) low cost and (3) high aggregate efficiency [7].

Numbers of strategies for synthesizing ZnO nanoparticles have been developed. ZnO nanoparticles can be fabricated using both classical methods such as combustion [8], thermal decomposition [9], sol-gel method [10], co-precipitation [11], and hydrothermal methods [12] and advanced methods such as ultrasonication [13], microwave-assisted combustion [14] , and green approaches [15]. Among the different synthesis techniques, the sol-gel method combined with ultrasound has been shown to be effective in reducing the size of small particles. Ultrasonic waves are showed to prevent the agglomeration of particles and break up agglomerates [16]. Therefore, in this study, we use sol-gel method combined with ultrasound to synthesize ZnO nanomaterials. Then, the material were applied as a photocatalyst to decompose methylene blue in aqueous solution.

* Corresponding author: thinh.nguyenngoc@hust.edu.vn
https://doi.org/10.15251/DJNB.2023.183.889

2. Experimental

2.1. Materials and method

All starting materials and solvent including zinc acetate ($Zn(CH_3COO)_2.2H_2O$), oxalic acid ($C_2H_2O_4.2H_2O$), and pure ethanol (C_2H_5OH) are in analytically grade.

The amount of 3.29 g $Zn(CH_3COO)_2.2H_2O$ was completely dissolved in 100 mL of C_2H_5OH in an ultrasonic bath (Elmasonic S100H Ultrasonic Bath) at 60 ^oC to form solution A. Similarly, the amount of 2.51 g of $C_2H_2O_4.2H_2O$ was completely dissolved in 60 mL of C_2H_5OH at 60 ^oC in the ultrasonic bath, resulting solution B. Slowly pour solution B into solution A on an ultrasonic bath at 60 °C until a gel mixture is formed. The final gel mixture was, then, dried at 80 ^oC for 12h. Finally, the materials were calcined at 400 ^oC, 500 ^oC, 600 ^oC, and 700 ^oC, with the residence time of 2 hours.

2.2. Characterization methods

The structural properties of the obtained ZnO nanoparticles were characterized by using a Bruker D8 advanced X-ray diffractometer with scanning rate of 0.02 s−1 and scanning range of 20–75°. The morphological properties of nanoparticles were characterized by using Hitachi S-4800 at 15 kV (the field emission scanning electron microscopy (FESEM) machine). Transmission electron microscopy (TEM) images of the material were captured with a JEOL JEM-1010 transmission electron microscope (acceleration voltage of 200 kV). The thermal stability and decomposition temperature of the materials were studied by thermal gravimetric analysis (TGA) (DSC131, LABSYS TG/DSC1600, TMA, and Setaram, France). The thermogravimetry (TG) curve was performed at the heating rate of 10°C/min from room temperature to 900°C.

2.3 Photocatalytic study

The photocatalytic activity was assessed as described in previous publications. [5] The amount of 0.1g of the synthesized ZnO nanoparticles was accurately weighted, dispersed in 100 mL of methylene blue solution. The mixture was left in the dark for 30 minutes to achieve adsorption equilibrium and uniform dispersion of particles. The photocatalysis was carried out under a closed system under the illumination of a 250W Osram high-pressure mercury lamp that acted as a source of ultraviolet light. After specified time intervals, a volume of 4 mL of the mixture was centrifuged to separate all the ZnO nanoparticles. The absorbance of methylene blue in the supernatant was measured at 664 nm light, using a UV-vis spectrophotometer (Agilent 8453).

The percentage of photocatalytic degradation was calculated using the equation:

$$Percentage\ photodegardation\ (R) = \frac{A_0 - A}{A_0} \times 100$$

where, A_o is initial absorbance of dye and A is absorbance of dye solution after UV light irradiation [5].

3. Results and discussion

3.1. Thermal analysis

In order to select the appropriate calcination temperature for the synthesis of ZnO nanoparticles, we used thermal analysis method. Figure 1 is the results of the thermal analysis of the gel synthesized according to the procedure in section 2.1.

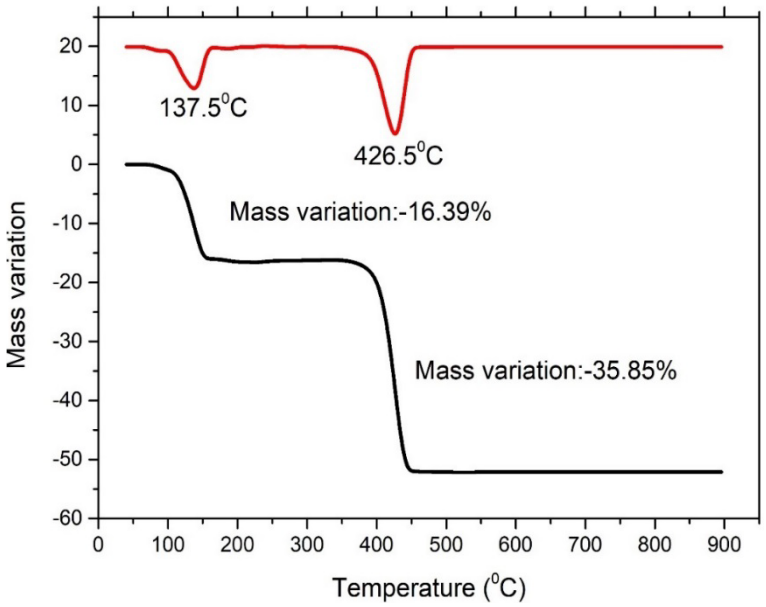

Fig. 1. The thermal analysis of the ZnC_2O_4 gel.

Accordingly, in the temperature range from 30 °C to 100 °C, there was no change in mass. This means that the ZnC_2O_4 gel is stable in this temperature range. In the temperature range from 100 °C to 200 °C, a decrease in mass is observed. The mass decreased by 16.3% in the temperature range of 100 °C to 200 °C. The cause of this mass reduction is probably due to the dehydration process. The next mass reduction effect is in the temperature range of 380 °C - 450 °C with a sharp decrease of 35.85%. The cause of this mass reduction is the decomposition of $C_2O_4^{2-}$. From 450 °C, the TG curve is stable. This result proves that the temperature of ZnO formation is about 400-450 °C. On that basis we choose the heating temperature of 400 °C, 500 °C, 600 °C, and 700 °C with the residence time is 2 hours. From the results of thermal analysis, it can be predicted that ZnO nanoparticles are formed according to the following reactions:

$$Zn(CH_3COO)_2.2H_2O + H_2C_2O_4.2H_2O \rightarrow ZnC_2O_4.2H_2O + 2CH_3COOH + 2H_2O \quad (1)$$

$$ZnC_2O_4.2H_2O + 1/2\ O_2 \rightarrow ZnO + 2CO_2 + 2H_2O \quad (2)$$

3.2. X-ray diffraction analysis

Figure 2 is the X-ray diffraction spectrum of ZnO nanoparticles obtained after calcination at 400 °C, 500 °C, 600 °C, and 700 °C. From the XRD diagram, we can see that in all the samples, there are characteristic peaks of ZnO with 2θ diffraction angle of 31.8°, 34.4°, 36.2°, 47.5°, 56.6°, 62.8°, 66.3°, 68.1° and 69.3° for the crystal face families (100), (002), (101), (102), (110), (103), (200), (112) and (201) of the hexagonal wurtzite ZnO, respectively (JCPDS No. 36-1451) [5,6,7]. It can be seen that the synthesized ZnO crystal is a hexagonal wurtzite crystal. This is the most common crystalline form and has the highest photocatalytic activity of ZnO. In the XRD spectra, no other diffraction peaks associated with any impurities were detected. This confirms the existence of ZnO in the crystalline phase with high purity.

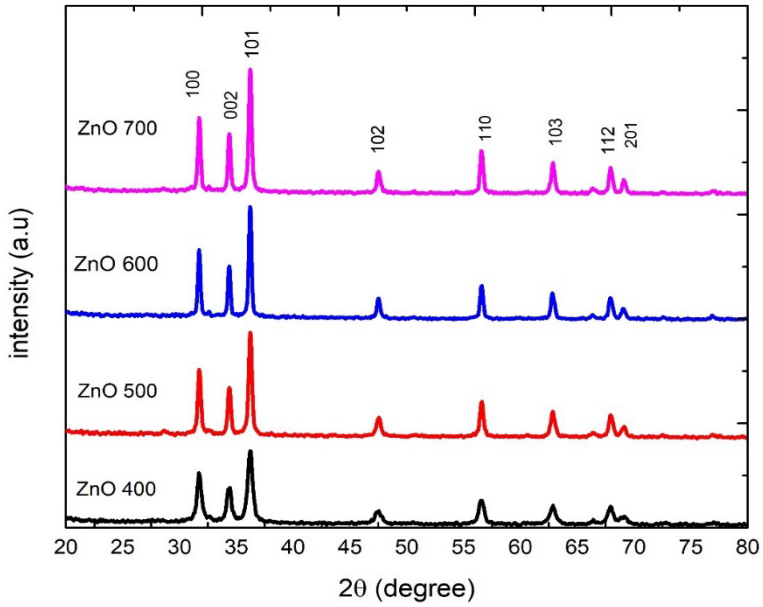

Fig. 2. X-ray diffraction spectra of ZnO nanoparticles obtained after calcination at 400 °C, 500 °C, 600 °C, and 700 °C.

In the case of the wurtzite phase, the lattice parameters (a,c, V) are calculated using the formula:

$$c = \frac{\lambda}{sin\theta_{(002)}}$$

$$a = \frac{\lambda}{\sqrt{3}\, sin\theta_{(100)}}$$

$$\frac{1}{d_{hkl}^2} = \frac{4}{3}\left[\frac{h^2 + hk + k^2}{a^2}\right] + \frac{l^2}{c^2}$$

where d is the distance between the lattice planes, λ = 1.54 A^0 is the wavelength of the X-ray radiation used, θ_{100} and θ_{002} are the angles of the diffraction peaks 100 and 002, respectively. The volume (V) of the unit cell for the hexagonal system is calculated using the equation:

$$V = 0.866 \times a^2 \times b$$

The average crystallite size of ZnO nanoparticles is calculated from the diffraction peak expansion according to the Debye–Scherer formula D=kλ/βcosθ, where D is the crystal size, k is constant (0.94), λ= 0.154 nm is the X-ray wavelength, β is the half-height peak width (FWHM) [7]. The average crystallite size of ZnO nanoparticles was calculated for the peak corresponding to the crystal face (101) because that is the peak with the greatest intensity and is not overlapped with other peaks. The obtained results on lattice parameters, basic lattice cell volume, and average crystallite size of ZnO nanocrystals are shown in Table 1.

Table 1. The lattice parameters and the average crystallite size of ZnO nanoparticles.

	a (Å)	c (Å)	c/a	Volume ($Å^3$)	D (nm)
JCPDS 36-1451	3.249	5.206	1.602	47.63	x
ZnO-400°C	3.254	5.202	1.598	47.70	21.76
ZnO-500°C	3.254	5.209	1.601	47.76	25.72
ZnO-600°C	3.251	5.213	1.603	47.71	31.42
ZnO-700°C	3.250	5.211	1.603	47.66	35.42

From Table 1, it can be seen that the network parameters of the synthesized ZnO nanoparticles are quite similar to those of the standard sample. In addition, as the calcination temperature increases, the average size of ZnO nanoparticles increases. It is possible that higher calcination temperature results in the agglomeration of particles to form larger sized particles.

3.3. FESEM analysis

Scanning electron microscopy (FESEM) results of ZnO nanocrystals calcined at different temperatures are shown in Figure 3. The spherical ZnO nanocrystals is clearly observed. The particles of the sample ZnO-400^{o}C are uniformly distributed and the smallest size is ~20-24 nm. For samples that obtained at higher calcination temperature, it can be seen that the particle size is larger and the size distribution is uneven (with some larger number of particles). This once again confirms the formation of agglomerates at high temperatures.

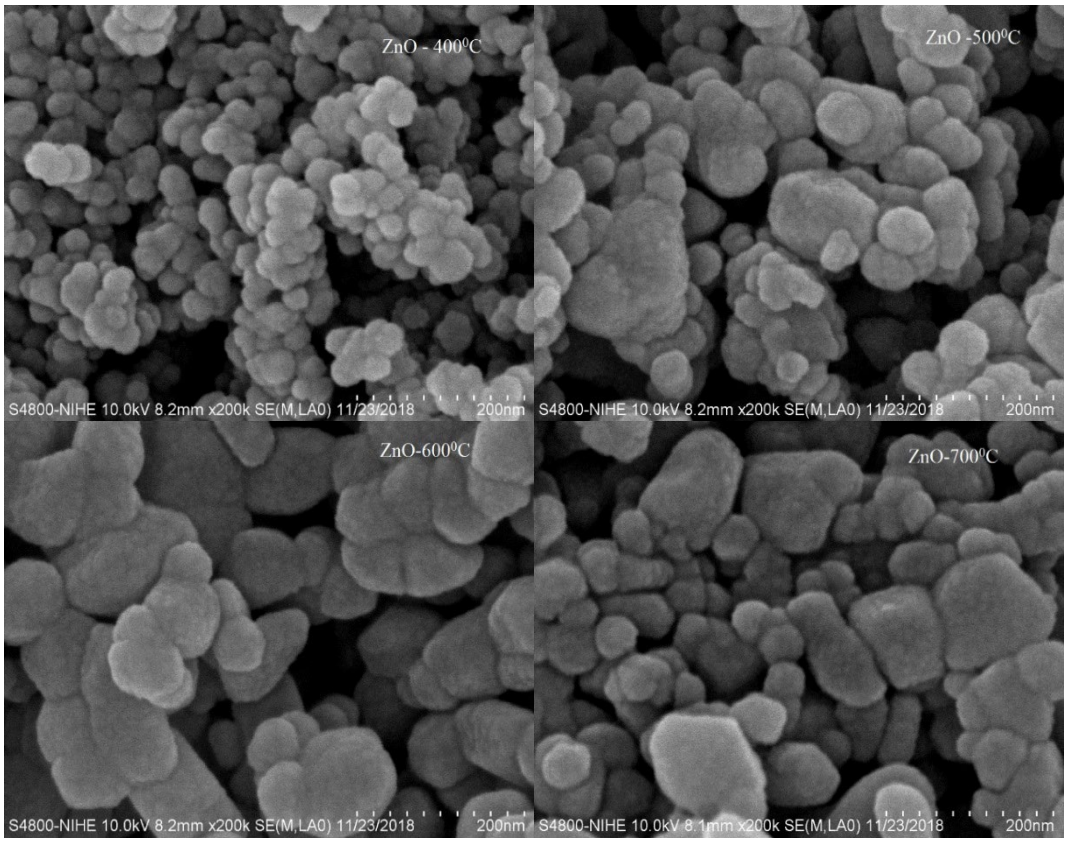

Fig. 3. FESEM images of ZnO nanoparticles obtained after calcination at 400 ^{o}C, 500 ^{o}C, 600 ^{o}C, and 700 ^{o}C.

3.4. TEM analysis

TEM scanning electron microscopy results of ZnO nanocrystals calcined at 600 ^{o}C are shown in Figure 4. ZnO nanoparticles can be seen as spherical and hexagonal shapes with the size of 25-30 nm.

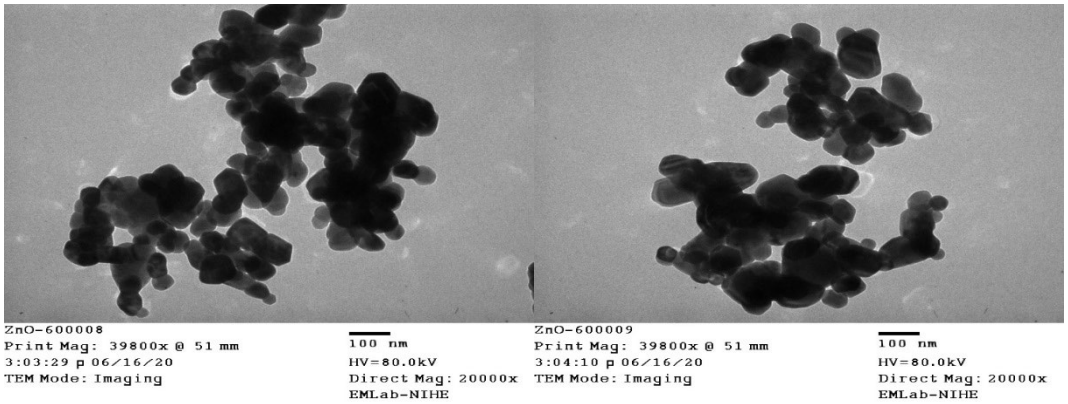

Fig. 4. TEM image of ZnO obtained after calcination at 600 °C.

3.5. UV Vis analysis

The UV Vis absorption spectrum of the ZnO nanoparticles (with the concentration of 0.01% in aqueous solution) is shown in Figure 5. All samples showed a single absorption peak (under 400 nm). For ZnO-400°C, ZnO-500°C, and ZnO-600°C samples, the absorption peaks are quite sharp, showing that the particle size distributions are more uniform than that of the ZnO-700°C sample. This consistent with the results of the FESEM analysis.

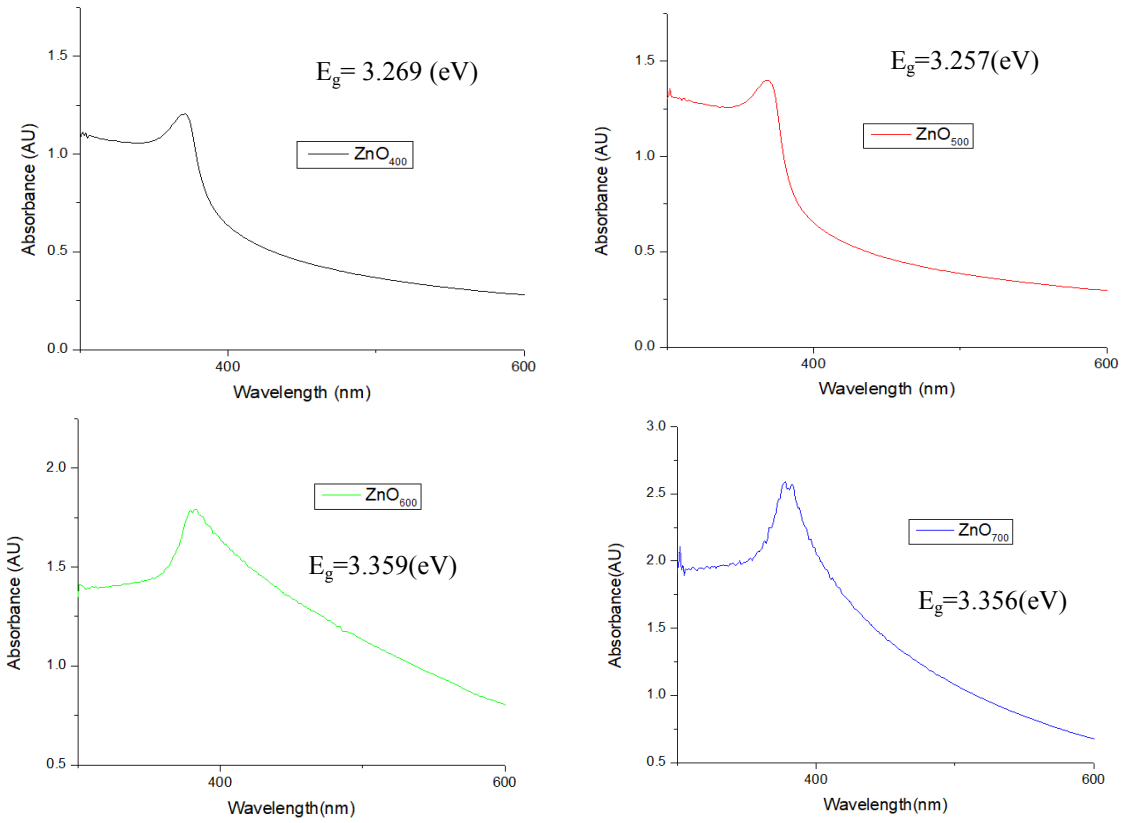

Fig. 5. UV Vis absorption spectrum of ZnO nanoparticles obtained after calcination at 400 °C, 500 °C, 600 °C, and 700 °C.

From the results of the UV Vis spectrum, the band gap energy E_g can be calculated according to the following formula [17]:

$$E_g = \frac{hc}{\lambda\max} = \frac{6.625\times10^{-34}Js\times3\times10^{8}ms^{-1}}{\lambda_{max}} = \frac{19.875\times10^{-26}}{\lambda_{max}}J = \frac{1242}{\lambda_{\max}(in\ nm)} = E_g(\text{eV})$$

The obtained E_g value are of 3.269; 3,257; 3,359 and 3,356 for ZnO-400^{o}C, ZnO-500^{o}C, ZnO-600^{o}C, and ZnO-700^{o}C samples, respectively

3.6. Photocatalytic analysis

The photocatalytic degradation of methylene blue over time is shown in Figure 6 and Figure 7. It can be seen that the synthesized ZnO nanoparticles can decompose 82 - 95.7% methylene blue within 40-50 minutes under UV light. The best degradation efficiency of methylene blue is performed by the ZnO-600^{o}C sample (96%) after 40 minutes, while the lower degradation efficiency of methylene blue of 92%, 89%, and 82% is obtained by ZnO-700^{o}C, ZnO-500^{o}C, and ZnO-400^{o}C samples, respectively, after 50 minutes.

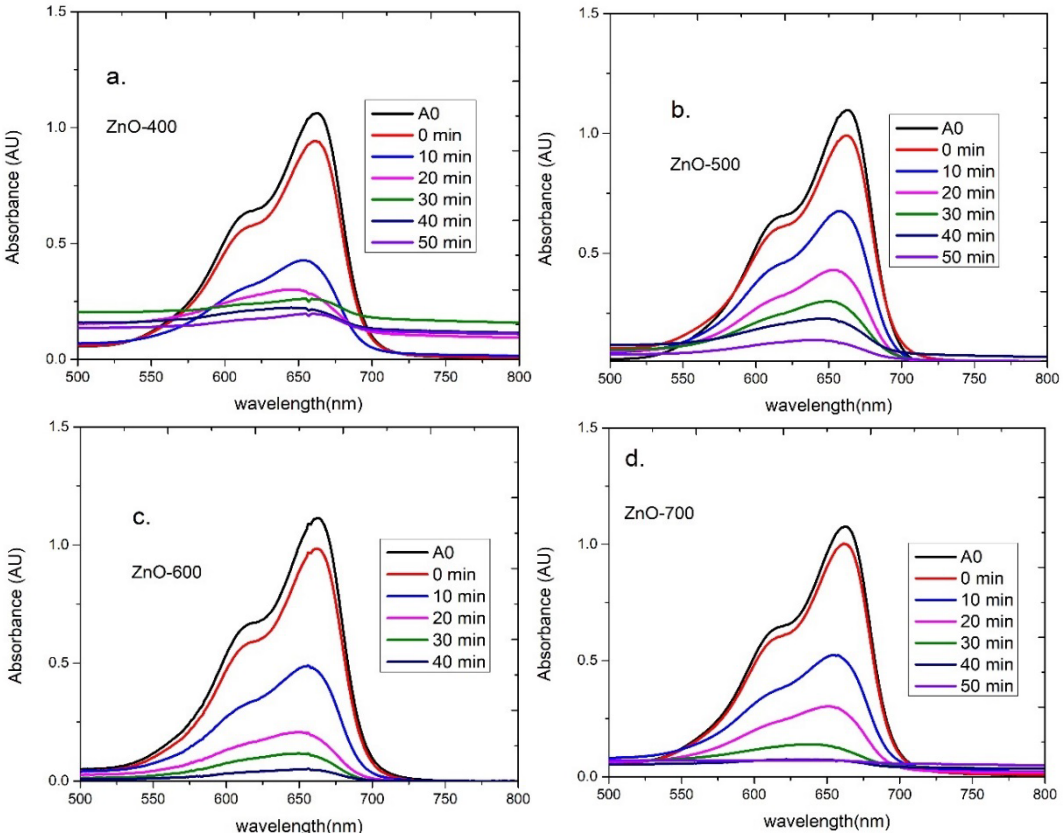

Fig. 6. UV-vis spectra of the mixture of methylene blue and ZnO-400^{o}C (a), ZnO-500^{o}C (b), ZnO-600^{o}C (c) và ZnO-700^{o}C (d) nanoparticles over time.

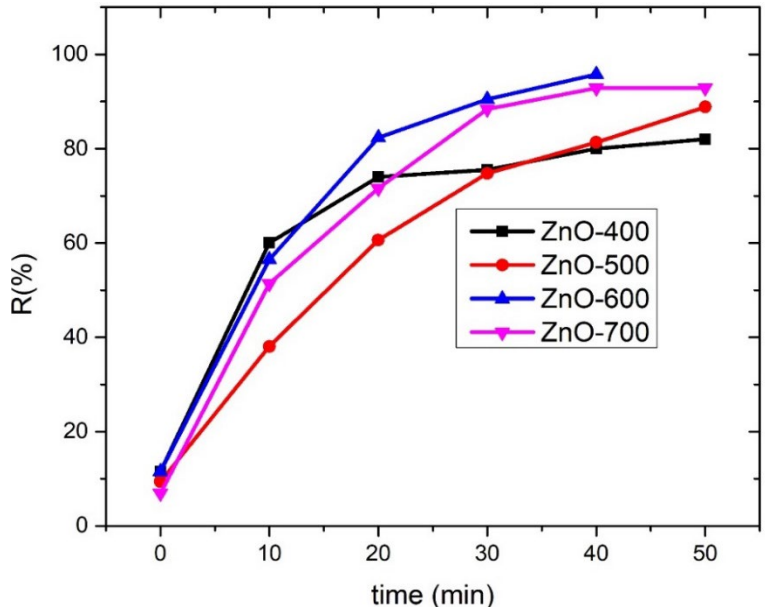

Fig. 7. The removal efficiency of methylene blue by ZnO nanoparticles under UV light.

4. Conclusion

In this study, nano-sized ZnO particles have been successfully synthesized by sol-gel method combined with ultrasound. From the XRD analysis results, the synthesized ZnO crystalline phase has a wurtzite hexagonal structure. The crystallite size of ZnO particles depends on the calcination temperature. The FE-SEM analysis results show that the ZnO nanomaterial particles have spherical and hexagonal shapes, with 20-30 nm in size. The synthesized ZnO nanomaterials have ability to decompose of methylene blue under UV light. Among samples, the ZnO-600^{o}C nanoparticles has the highest removal efficiency (more than 96% of methylene blue is decomposed after 40 minutes).

References

[1] N.Hossain, M. A. Islam, M. A. Chowdhury, A. Alam, Applied Surface Science Advances, **12**, 100341 (2022); https://doi.org/10.1016/j.apsadv.2022.100341
[2] G. Magesh, G. Bhoopathi, N. Nithya, A.P. Arun, E. Ranjith Kumar, , Superlattices and Microstructures, **117**, 36-45 (2018); https://doi.org/10.1016/j.spmi.2018.03.003
[3] M. Hafiz, A. Hassanein, M. Talhami, M. AL-Ejji, M. K. Hassan, A. H. Hawari, . Journal of Environmental Chemical Engineering, **10** (6), 108955, (2022); https://doi.org/10.1016/j.jece.2022.108955.
[4] N.T. Nguyen, V.A. Nguyen, T.H. Nguyen, Journal of Dispersion Science and Technology, (2022); https://doi.org/10.1080/01932691.2022.2063885
[5] N.T. Nguyen, V.A. Nguyen, Journal of Nanomaterials, (2020); https://doi.org/10.1155/2020/1768371
[6] Y.M Chen, J. Gao, Materials Letters: X, **12**, 100106 (2021); https://doi.org/10.1016/j.mlblux.2021.100106.
[7] C. Tian, Q. Zhang, A. Wua M.Jiang, Z. Liang, B. Jiang and H. Fu, Chem. Commun., **48**, 2858-2860 (2012); https://doi.org/10.1039/C2CC16434E
[8] P. Sathish, N. Dineshbabu, K. Ravichandran, T. Arun, P. Karuppasamy, M. SenthilPandian, P. Ramasamy, Ceramics International, **47**, (19), 2021; https://doi.org/10.1016/j.ceramint.2021.06.224.
[9] R. Rathore, N. Kaurav, Materials Today: Proceedings, **54**, Part 3, (2022);

https://doi.org/10.1016/j.matpr.2021.10.207.
[10] T.Ahmad, V. Pandey, M. S. Husain, Adiba, S. Munjal, Materials Today: Proceedings, **49**, Part 5,(2022); https://doi.org/10.1016/j.matpr.2021.07.456.
[11] E. Indrajith Naik, H.S. Bhojya Naik, M.S. Sarvajith, E. Pradeepa, Inorganic Chemistry Communications, **130**, 108678, (2021); https://doi.org/10.1016/j.inoche.2021.108678.
[12] U. T. Nakate, Y.T. Yu, S. Park, Ceramics International, **48**, (19), Part B, (2022); https://doi.org/10.1016/j.ceramint.2022.03.017.
[13] S. Selvinsimpson, P. Gnanamozhi, V. Pandiyan, M. Govindasamy, M. A. Habila, N. AlMasoud, Y. Chen, Environmental Research, **197**, 111115, (2021); https://doi.org/10.1016/j.envres.2021.111115.
[14] E.D. Sherly, J. J. Vijaya, N. S. Selvam, L. J. Kennedy, Ceramics International, **40**, 4, (2014); https://doi.org/10.1016/j.ceramint.2013.11.006.
[15] T. S. Aldeen, H. E. A. Mohamed, M. Maaza, Journal of Physics and Chemistry of Solids, **160**, 110313, (2022); https://doi.org/10.1016/j.jpcs.2021.110313.
[16] C.Bogatu, D.Perniu, C. Sau, O.Iorga, M. Cosnita, A. Duta, Ceramics International, **43**, 11, (2017); https://doi.org/10.1016/j.ceramint.2017.03.054.
[17] R. Kumar, G. Kumar, M.S. Akhtar, A. Umar, Journal of Alloys and Compounds, **629**, 2015; https://doi.org/10.1016/j.jallcom.2014.12.232.